Evidence of silicate immiscibility within flood basalts from the Central Atlantic Magmatic Province

J. G. Shellnutt

Department of Earth Sciences, National Taiwan Normal University, 88 Tingzhou Rd., Section 4, Taipei 11677, Taiwan (jgshelln@ntnu.edu.tw)

J. Dostal

Department of Geology, Saint Mary's University, Halifax, Nova Scotia, Canada

Y. Iizuka

Institute of Earth Sciences, Academia Sinica, Taipei, Taiwan

[1] The role silicate-liquid immiscibility plays in the formation of macro-scale, bimodal volcanic/plutonic igneous complexes, and Fe-Ti oxide deposits is debated as the rock compositions produced by immiscibility are similar to those produced by other petrological processes. Within the flows of the North Mountain basalt of the Central Atlantic Magmatic Province are centimeter-thick granophyre layers. The granophyre layers are a mixture of mafic (i.e., ilmenite, magnetite, ferroaugite, plagioclase, stilpnomelane, ferrorichterite) and felsic (i.e., sanidine, quartz) minerals and highly siliceous (>75 wt% SiO_2) mesostases. Petrological modeling indicates that the siliceous mesostasis + sanidine + quartz $\pm$ ferrorichterite represents a Si-rich silicate immiscible melt whereas the ferroaugite + plagioclase + stilpnomelane represent the Fe-rich silicate immiscible liquid. The identification of naturally occurring silicate-liquid immiscibility at scales greater than micron level is an important observation which may be useful in identifying volcanic and plutonic rocks which formed by macro-scale silicate-liquid immiscibility.

1. Introduction

[2] Silicate-liquid immiscibility or "magma unmixing" is postulated as a possible process for the development of cogenetic suites of basic and acidic igneous rocks in ophiolites and continental volcanic-plutonic complexes [*Dixon and Rutherford*, 1979; *Eby*, 1980; *Ferreira et al.*, 1994; *Jakobson et al.*,

2005; *Veksler et al.*, 2007; *Namur et al.*, 2011; *Charlier et al.*, 2011; *Charlier and Grove*, 2012]. Experimental studies and micron-scale petrographical evidence of silicate-liquid immiscibility are documented within lunar and terrestrial igneous rocks but whether or not large-scale bimodal volcanic/plutonic complexes and Fe-Ti oxide deposits can form by silicate-liquid immiscibility in nature is uncertain [*Roedder*, 1951, 1979; *Roedder and Weiblan*, 1970; *Watson*, 1976; *Philpotts*, 1976, 1982; *Duchesne*, 1999]. The main problem identifying igneous rocks produced by silicate-liquid immiscibility is that their major element compositions are similar to rocks produced by other petrological processes (e.g., fractional crystallization, partial melting) although rocks produced by silicate-liquid immiscibility are expected to have very different trace element abundances [*Watson*, 1976; *Roedder*, 1978, 1979]. In basaltic systems, water tends to suppress plagioclase crystallization while promoting Fe-Ti oxide crystallization thus preventing Fe-enrichment in the residual liquid and reducing the likelihood that the field of silicate-liquid immiscibility will form [*Charlier and Grove*, 2012]. Nonetheless, silicate-liquid immiscibility is considered to be an important process during the formation of some layered intrusions (i.e., Skaergaard, Sept Iles, Panzhihua) and possibly contributed to the development of oxide-ore deposits but this remains disputed [*Philpotts*, 1967; *McBirney*, 1975; *Kolker*, 1982; *Duchesne*, 1999; *Jakobsen et al.*, 2005; *Charlier et al.*, 2011; *Shellnutt et al.*, 2011; *Charlier and Grove*, 2012; *Zhou et al.*, 2013].

[3] After an early, extensive period of crystal fractionation, a mafic tholeiitic or alkalic magma may enter the two silicate immiscibility field of the $K_2O-FeO-Al_2O_3-SiO_2$ phase diagram [*Roedder*, 1951; *Philpotts*, 1976, 1979, 1982]. The experimental results show that the high field strength cations (i.e., P, REE, Ta, Ti, Mn, Mg, Sr, and Ba) will partition into the less polymerized Fe-rich silicate immiscible melt rather than the Si-rich melt [*Watson*, 1976; *Ryerson and Hess*, 1978; *Veksler et al.*, 2006], a situation which is nearly the opposite of crystal fractionation. The extent to which silicate immiscibility can be identified in terrestrial plutonic rocks may be more difficult than their volcanic counterparts considering the difference in cooling rates. In fact other magmatic processes in plutonic rocks may "overprint" features of immiscibility, such as: gravitation settling, equilibrium/fractional crystallization or layering processes (i.e., double diffusion) which may not be as efficient in lavas as they are in magma chambers.

[4] One of the best localities to study silicate-liquid immiscibility within volcanic rocks is the North Mountain basalt of the Central Atlantic Magmatic Province (CAMP) in Nova Scotia. Nearly a hundred years ago, *Bowen* [1916] cited the North Mountain basalts as an example of differentiation of mafic magmas which was based on the work by *Powers and Lane* [1916] and *Powers* [1916]. Studies by *Greenough and Dostal* [1992a, 1992b], *Dostal and Greenough* [1992], *Kontak et al.* [2002], and *Kontak and Dostal* [2010] have shown that there are centimeter-thick granophyric layers or pipes within the upper flows of the North Mountain basalts. *Kontak et al.* [2002] identified petrographic evidence (i.e., ocelli) of silicate-liquid immiscibility in the North Mountain basalt thus it is possible that the granophyre may represent a larger scale expression of immiscibility than the previously identified "micron-scale" evidence. Furthermore, *Philpotts* [1979] and *Philpotts and Doyle* [1983] identified silicic mesostases within CAMP basalts from Connecticut as being produced by silicate-liquid immiscibility. In this paper, we present new mineral chemistry, whole rock elemental and isotope data of the granophyric layers within the basalt flow in order to determine whether or not the differentiation that occurred in the North Mountain basalt can be attributed, in part or wholly, to silicate-liquid immiscibility.

2. Geological Background

[5] North Mountain basalts (NMB) of Nova Scotia form the northernmost part (with an exception of the Avalon dike of Newfoundland) of the early Mesozoic Central Atlantic Magmatic Province (CAMP). CAMP tholeiites crop out along the eastern margin of the North America from South Carolina to Nova Scotia and Newfoundland (Figure 1). The rocks are related to an extensive magmatic event which took place at ~200 Ma [*Hodych and Dunning*, 1992; *Kontak and Archibald*, 2003] and lasted for 580 ka [*Olsen*, 1997; *Olsen et al.*, 1998; *Kontak*, 2008; *Jourdan et al.*, 2009]. The magmatic activities were connected with lithospheric extension associated with the initial stages of the opening of the Atlantic Ocean. The North Mountain basalts were emplaced in the Bay of Fundy graben that runs parallel to the continental margin of North America. The lava flows crop out for about 200 km along the southeastern shore of the Bay of Fundy and are also exposed along the north shore of the Bay of Fundy in the Minas basin and Grand Manan Island [*McHone et al.*,
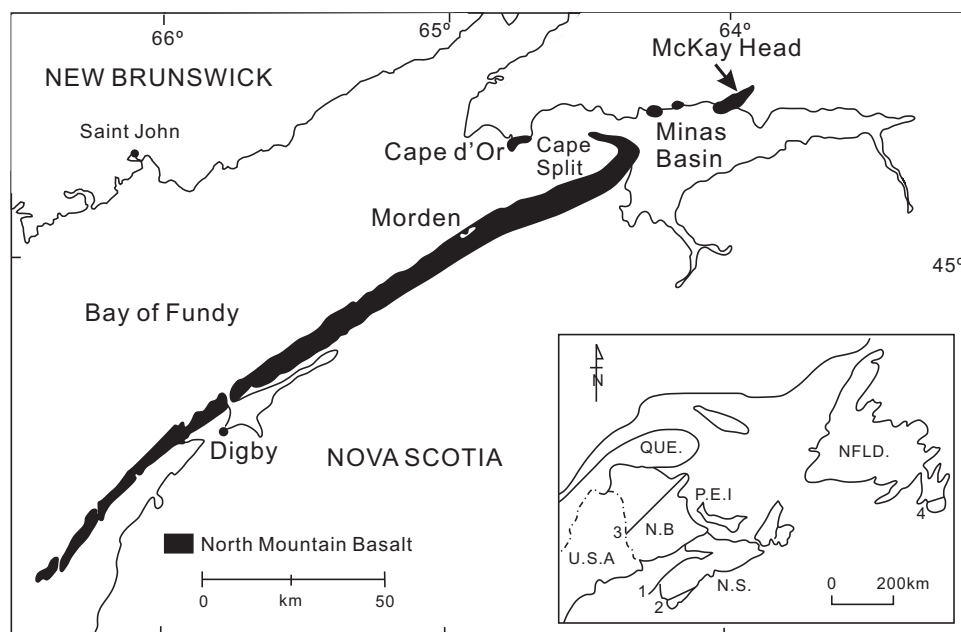
Figure 1. Location of the McKay Head volcanic section and the North Mountain basalt. Inset map of Atlantic Canada showing the distribution of CAMP-related mafic volcanic and intrusive rocks. 1—North Mountain basalt, 2—Shelburne Dyke, 3—Caraquet Dyke, 4—Avalon Dyke (modified from *Dostal and Greenough* [1992]).

2005] and probably underlie most of the Bay of Fundy covering an area of about 10,000 km² [*Dostal and Dupuy*, 1984; *Greenough and Papezik*, 1987]. The thickness of the NMB decreases from the southwest (∼400 m around Digby) to the northeast (∼275 m near Cape Split) [*Papezik et al.*, 1988]. The subaerial basalts were emplaced just above the Triassic-Jurassic boundary [*Olsen et al.*, 1987] and conformably overlie the Mesozoic continental sedimentary rocks which lie unconformably on Carboniferous and older rocks. The basalts are in turn unconformably overlain by Mesozoic sediments.

[6] According to the superposition, geochemical data and nature of the flows, the NMB is usually subdivided into three units: the lower massive flow (∼40–185 m thick), the middle amygdaloidal flows (several flows up to 20 m thick, totaling ∼9–165 m) and the upper massive unit (1–2 flows, totaling 9–165 m) [*Kontak et al.*, 2005]. The lower and upper units are composed of massive basalts with microcrysts of plagioclase and pyroxene (augite ≫ pigeonite) with variable amounts of mesostases. The upper unit has typically higher contents of mesostases than the lower unit and contains pegmatitic layers [*Greenough and Dostal*, 1992a, 1992b]. The mafic pegmatitic (i.e., 2–4 mm long crystals) layers are ∼10–∼60 cm in thickness

and interlayered with ∼80–180 cm thick coarse grained (i.e., 1.5–2 mm long crystals) basalts [*Greenough and Dostal*, 1992b]. In the middle of the pegmatitic layers are 1–4 cm thick, fine grained, sinuous granophyric layers which form sharp contacts with the pegmatite. The middle unit is readily recognizable due to numerous amygdules and vesicles and resembles recent pahoehoe flows [*Kontak et al.*, 2005]. The basalts are fine grained and massive when not strongly vesiculated. There are also some regional variations where by the basalts from southwestern part at Digby area are more mafic than those from around Cape Split. In addition to chemistry [*Dostal and Greenough*, 1992], these regional variations are also observed in mineralogy. The clinopyroxenes are more abundant and coarser at the southwestern part where orthopyroxene is also present compared to the northeastern part [*Kontak et al.*, 2005].

[7] Geochemistry of North Mountain basalts show that the rocks are quartz-normative continental tholeiites which were affected by crustal contamination probably within the lower crust [*Dostal and Dupuy*, 1984]. The basalts have been inferred to be derived from subcontinental lithospheric mantle within the spinel stability field [*Dupuy and Dostal*, 1984; *Murphy and Dostal*, 2007; *Murphy et al.*, 2011].

3. Methods

3.1. Electron Probe Microanalysis

[8] A mineralogical investigation was carried out by a field emission electron probe micro analyzer (JEOL EPMA JXA-8500F) equipped with five wave-length dispersive spectrometers (WDS) at the Institute of Earth Sciences, Academia Sinica in Taipei. Secondary and backscattered electron images were used to guide the analysis on target positions of minerals. A 2 μm defocused beam was operated for analysis at an acceleration voltage of 12 kV with a beam current of 6 nA. The measured X-ray intensities were corrected by the ZAF method using the standard calibration of synthetic standards with various diffracting crystals, as follows: wollastonite for Si with TAP crystal, corundum for Al (TAP), Cr-oxide for Cr with PET crystal, hematite for Fe with LiF crystal, Mn-oxide for Mn (PET), periclase for Mg (TAP), Ni-oxide for Ni (LiF), wollastonite for Ca (PETH), albite for Na (TAP), orthoclase for K (PET), apatite for P (PET), and fluorite for F (TAP). The X-ray peak counting times for the upper and lower baselines of each element were 10 s and 5 s, respectively. Standards run as unknowns yielded relative standard deviations of <2% for F and P, <1% for Si, Na, and K, and <0.5% for other elements. Detection limits were <0.5 wt% for F and P and <5–600 ppm for other elements. The complete data set is located in supporting information Table S1[1].

3.2. Wavelength Dispersive X-ray Fluorescence

[9] Rock samples were cut into small pieces using a diamond-bonded steel saw and were then crushed in a steel jaw crusher. The crusher was extensively cleaned after each sample with deionized water. The crushed samples were pulverized in an agate mill until the suitable particle size was obtained. The samples were then heated to temperatures of 110°C and 900°C, respectively, to determine loss on ignition (LOI). Lithium metaborate was added to the oxidized samples and fused to produce a glass disc using a Claisse M4 fluxer. The major oxide concentrations were determined by WD-XRFS using a PANalytical Axios mAX spectrometer at National Taiwan Normal University in Taipei. The accuracy of the XRF analyses are estimated to be ±2% for major oxides which are present in concentrations >0.5%.

3.3. ICP-MS Trace Element Geochemistry

[10] All trace elements were analyzed using an Agilent 7500cx inductively coupled plasma mass spectrometer (ICP-MS) at National Taiwan University, Taipei, Taiwan. Approximately 20 mg of powder from each sample was digested in a Teflon beaker using a combination of HF, HNO_3, and HCl. Initially, samples were heated in closed beakers with HF and HNO_3 for at least 2 days and then dried. Two milliliters of 6 N HCl was added to each sample and then left to dry. This step was repeated. An additional 2 ml of 1 N HCl was added to each sample and then the sample was centrifuged. The supernatant was extracted from each beaker into a new one. If there was solid residue left in the beakers then the procedure was repeated until all samples were fully digested. Samples were diluted using 2% HNO_3 and an Rh and Bi spike was added for the internal standard. The standard reference material used for this study is AGV-2 (andesite), BCR-2 (basalt), BIR-1 (basalt), and DNC-1 (dolerite). The precision for the trace element results are better than ±5%.

3.4. Thermal Ionization Mass Spectrometry

[11] Approximately 75–100 mg of whole-rock powder was dissolved using a mixture of HF-$HClO_4$ in a Teflon beaker at ~100°C. In many cases, the same procedures were repeated to ensure the total dissolution of the sample. Strontium and REEs were separated using polyethylene columns with a 5 ml resin bed of AG 50W-X8, 200–400 mesh. Neodymium was separated from other REEs using polyethylene columns with an Ln resin as a cation exchange medium. Strontium was loaded on a single Ta-filament with H_3PO_4 and Nd was loaded with H_3PO_4 on a Re-double-filament. $^{143}Nd/^{144}Nd$ ratios were normalized to $^{146}Nd/^{144}Nd = 0.7219$ and $^{87}Sr/^{86}Sr$ ratios to $^{86}Sr/^{88}Sr = 0.1194$. The Sr isotopic ratios were measured using a Finnigan MAT-262 thermal ionization mass spectrometer (TIMS) whereas the Nd isotopic ratios were measured using a Finnigan Triton TIMS in the Mass Spectrometry Laboratory, Institute of Earth Sciences, Academia Sinica, Taipei. The $2\sigma_m$ values for all samples are less than or equal to 0.000010 for $^{87}Sr/^{86}Sr$ and less than or equal to 0.000007 for $^{143}Nd/^{144}Nd$. The measured isotopic ratios for JMC Nd standard is 0.511813 ± 0.000010 $(2\sigma_m)$ and NBS987-Sr is 0.710248 ± 0.00001 $(2\sigma_m)$. The complete data set is in supporting information Table S2.

---

[1]Additional Supporting Information may be found in the online version of this article.

4. Results

4.1. Electron Probe Micro Analysis

[12] The granophyric layers are fine-grained (<0.5 mm) and contain granular plagioclase, alkali feldspar, and acicular quartz. There are a number of mafic minerals in the layers including subhedral to anhedral magnetite and ilmenite, stilpnomelane, ferrorichterite, ferroaugite, and accessory amounts of apatite. The plagioclase ranges in composition from An_{56} to An_{33} although two crystals from MH12-001 samples have oligoclase (i.e., An_{18-19}) compositions. The alkali feldspar is sanidine and has compositions of $An_{1-3}Ab_{30-57}Or_{40-69}$. The two pyroxenes identified are augite and ferroaugite. The augite ($Wo_{33-38}En_{31-38}Fs_{25-36}$) has higher magnesium, aluminum ($Al_2O_3 = 1.3$ wt% to 1.7 wt%) and titanium ($TiO_2 = 0.7$ wt% to 1.1 wt%) and lower iron and calcium than the ferroaugite ($Wo_{38-40}En_{10-18}Fs_{44-50}$; $Al_2O_3 = 0.4$ wt% to 0.7 wt%; $TiO_2 = 0.3$ wt% to 0.8 wt%). The magnetites contain between 5.4 wt% and 12.8 wt% TiO_2 and can be classified as titanomagnetite. The ilmenite contains between 35.4 wt% and 51.1 wt% total iron and 45.0 wt% to 56.2 wt% TiO_2. The MnO content is variable (MnO = 0.5 wt% to 12.9 wt%) whereas the MgO content is <1.5 wt%. The apatites are fluorine-rich.

[13] Interstitial to the plagioclase and pyroxene crystals is a microcrystalline, tan colored siliceous mesostasis [Greenough and Dostal, 1992a]. The mesostasis are amorphous and have a wide range in composition (Table 1). The most "primitive" mesostasis analyzed (i.e., C2-59) has 72.7 wt% SiO_2 whereas the most evolved mesostasis contains 88.2 wt% SiO_2 but even higher values ($SiO_2 > 90$ wt%) are reported by Kontak and Dostal [2010]. The alkalis and alumina decrease with increasing SiO_2 whereas TiO_2 (i.e., 0.01–0.13 wt%) and FeOt (i.e., 0.37–0.97 wt%) are nearly constant and show no discernible trends with respect to SiO_2. The remaining major elements have either very low abundances (i.e., MgO and MnO) or are variable (i.e., CaO and P_2O_5). The full mineral and mesostasis chemistry can be found in supporting information (Table S1).

4.2. Whole Rock Elemental and Isotope Data

[14] The granophyre layers collected from the North Mountain basalt at McKay Head for this study are moderately silicic (i.e., $SiO_2 = 57.5$ wt% to 60.3 wt.%), metaluminous (i.e., Al/Na + Ca + K < 1, Na + K/Al < 1) and have low to moderate Mg# of

Table 1. Major Element Compositions of the Basalt From McKay Head, Siliceous Mesostases, and Si-Rich Immiscible Liquids[a]

Sample		MH12-001						MH12-002			MH12-004				13	13	
Type	Basalt	Meso	Meso	Meso	Meso	Meso	Meso	Meso	Meso	Meso	Meso	Meso	Meso	Meso	Basalt	Si-L	Recalc
Spot	MCK1	A-5	A-6	A-11	B-50	C-53	C-54	C2-58	C2-59	C2-60	A2-12	A2-19	A2-20	A2-24			
Ref.	MH	MH	MH	MH	MH	MH	MH	MH	MH	MH	MH	MH	MH	MH	P82	P82	
SiO_2 (wt%)	51.00	87.29	82.49	81.84	86.64	78.78	87.75	88.18	72.70	77.57	80.04	77.97	81.5	83.06	50.36	72.8	72.01
TiO_2	1.40	0.10	0.12	0.10	0.0	0.01	0.08	0.12	0.10	0.13	0.09	0.09	0.06	0.0	1.06	0.8	0.80
Al_2O_3	14.60	7.74	9.62	8.94	7.76	9.14	7.28	4.81	14.00	10.38	9.17	10.23	8.13	6.93	14.51	12.5	13.87
Fe_2O_3t	10.62																
FeOt		0.82	0.50	0.57	0.37	0.43	0.40	0.84	0.97	0.86	0.79	0.74	0.71	0.43	8.09	3.1	2.97
MnO	0.22	0.12	0.0	0.0	0.0	0.09	0.05	0.0	0.0	0.0	0.05	0.04	0.0	0.0	0.12	0.0	0
MgO	6.50	0.0	0.0	0.0	0.02	0.0	0.02	0.0	0.0	0.0	0.04	0.05	0.04	0.05	6.26	0.0	0
CaO	9.16	0.94	1.06	1.03	1.63	1.11	1.00	0.23	0.49	0.17	0.13	0.15	0.18	0.26	10.77	1.2	0.49
Na_2O	2.52	2.75	3.60	3.60	2.72	2.01	2.52	1.34	4.50	2.44	2.11	1.72	1.84	2.01	2.48	2.7	4.46
K_2O	0.82	0.86	2.08	0.91	0.21	4.78	0.35	2.52	6.23	6.85	5.18	6.17	4.60	2.83	0.99	5.1	6.17
P_2O_5	0.13	0.09	0.0	0.0	0.0	1.11	0.0	0.01	0.04	0.01	0.04	0.08	0.04	0.01	0.45	0.1	0.04
LOI	2.30														2.37		
Total	99.27	100.8	99.52	97.05	99.38	97.50	99.49	98.14	99.14	98.51	97.73	97.3	97.17	95.62	97.46	98.3	100

[a]Type: Meso, mesostasis; Si-L, Si-rich immiscible liquid; MH, McKay Head; P82, data from Philpotts [1982]. LOI, loss on ignition. Recalc is the back calculated composition of C2-59 assuming Fe and Ti are similar to 13.

39 to 41 (Mg# = [Mg^{2+}/(Mg^{2+} + Fe^{2+}) $\times$ 100]). The whole rock major and trace elemental compositions of the granophyres fall within the andesite field of classification diagrams (Table 2). The chondrite normalized rare earth element patterns of the silicic rocks show light REE enrichment (La/Yb$_N$ = 4.9 to 5.4) and slightly negative Eu-anomalies (Eu/Eu* = 0.75–0.81) whereas the primitive mantle normalized plots show depletion of Ba, Nb, Sr, and Ti [*Sun and McDonough*, 1989]. The composition of the granophyres from this study is slightly more mafic than those reported by *Greenough and Dostal* [1992b] (Figure 2).

[15] The Sr-Nd isotope analyses are calculated to their initial values based on the reported ^{40}Ar-^{39}Ar ages (i.e., ~200 Ma) of the North Mountain basalt [*Jourdan et al.*, 2009]. The granophyres have initial ^{87}Sr/^{86}Sr values ranging from 0.70613 to 0.70627. The calculated induce error in the I$_{Sr}$ values is negligible (i.e., <0.00010) suggesting that Rb-Sr mobility is not a significant concern and thus the samples were not affected by hydrothermal alternation [*Jahn*, 2004]. The initial ^{143}Nd/^{144}Nd ratios for the rocks, similar to the I$_{Sr}$ values, are uniform (^{143}Nd/^{144}Nd = 0.51229 to 0.51231). Their εNd$_{(T)}$ values fall between −1.5 and −1.7 and have Proterozoic (1413–1468 Ma) depleted-mantle-based model ages (T$_{DM}$). The isotope data can be found in supporting information (Table S2).

5. MELTS Modeling

[16] The petrological evolution of magmas can be modeled using the program pHMELTS [*Ghiorso and Sack*, 1995; *Smith and Asimow*, 2005]. pHMELTS and its derivative software are calibrated to the SiO$_2$-TiO$_2$-Al$_2$O$_3$-Fe$_2$O$_3$-Cr$_2$O$_3$-FeO-MnO-MgO-CaO-Na$_2$O-K$_2$O-P$_2$O$_5$-H$_2$O system. The software allows the user to control intrinsic thermodynamic parameters such as pressure (bars), water (wt%) content and the relative oxidation state ($\times$O$_2$) of the magma that is being modeled. Here we model fractional crystallization of three compositions: (1) basalt from McKay Head, (2) siliceous mesostasis from the granophyre (C2-59), and (3) a Si-rich immiscible liquid composition reported by *Philpotts* [1982] in order to assess the chemical evolution of the liquids that are produced.

5.1. McKay Head Basalt Models

[17] For this study, the basalt at McKay Head (i.e., MCK1) reported by *Greenough and Dostal* [1992a] was selected as representative of the

volcanic rocks which erupted in the area. Sample MCK1 is typical of the continental tholeiites at McKay Head and within the upper flow of the North Mountain basalt [*Dostal and Greenough*, 1992; *Greenough and Dostal*, 1992a]. The primary purpose of the basalt modeling is to determine if it can produce compositions equal to the pegmatite layers found within the volcanic pile. The modeling conditions are low pressure (i.e., 1 bar), water content of ~0.5 wt% and a relative oxidation state equal to the FMQ (fayalite-magnetite-quartz) buffer. The relative oxidation state of the basalt was determined using the Fe^{3+}/Fe^{2+} ratio method of *Kress and Carmichael* [1991] assuming a low pressure (i.e., 1 bar) and eruption temperature of 1150°C.

[18] The modeling results show that olivine (Fo$_{79}$) and plagioclase (An$_{72}$) are the first minerals to crystallize when the temperature reaches 1170°C but by the time the temperature drops to 1150°C the olivine has stopped crystallizing (i.e., the rock is silica oversaturated) and is replaced by clinopyroxene (i.e., augite) as the only mafic silicate mineral whereas plagioclase (An$_{68}$) continues to crystallize at ever decreasing An content. Magnetite-structured titanium-rich spinel then crystallizes as temperatures reach 1090°C. The residual liquid composition of the model actually matches the bulk composition of the pegmatite layers when the temperature reaches 1140–1150°C which equals ~30% crystallization (Figure 2).

5.2. Siliceous Mesostasis Model

[19] We selected sample C2-59 from Table 1 to model because it is the most "primitive" sample of the siliceous mesostasis and best resembles the Si-rich immiscible silicate-liquid reported by *Philpotts* [1982]. We use the same pressure and oxidation state as the basalt models but we choose to run the models at anhydrous conditions because there is no indication of the bulk water content of the mesostasis. The modeling results show that alkali feldspar (i.e., An$_1$Ab$_{47}$Or$_{52}$) dominates the early to middle crystallization history as it is the only mineral to crystallize from 1070°C to 940°C (i.e., ~50% crystallization). Quartz begins to crystallize at 930°C followed by titanomagnetite at 910°C and fayalite (Fo$_0$) at 900°C.

5.3. Silicic Immiscible Liquid Model

[20] The Si-rich immiscible silicate-liquid 13 from Table 1 was selected because it resembles mesostasis sample C2-59 and its parental magma

Table 2. Major and Trace Elemental Data of the Granophyre From McKay Head[a]

Sample	MH12-001	MH12-002	MH12-003	MH12-004	SDC-1 m.v.	SDC-1 r.v.	AGV-2 m.v. (2)	AGV-2 r.v.	BCR-2 m.v. (2)	BCR-2 r.v.	BHVO-2 m.v. (2)	BHVO-2 r.v.	BIR-2 m.v. (2)	BIR-2 r.v.	DNC-1 m.v. (2)	DNC-1 r.v.
SiO_2 (wt%)	58.44	59.09	60.26	57.55	65.68	65.85										
TiO_2	1.97	1.37	1.23	1.70	0.99	1.01										
Al_2O_3	11.21	10.92	11.07	11.34	15.88	15.75										
Fe_2O_3t	13.37	13.26	12.28	13.74	6.76	6.90										
MnO	0.25	0.20	0.20	0.22	0.12	0.11										
MgO	4.31	4.63	4.30	4.61	1.68	1.69										
CaO	3.26	3.41	3.67	3.43	1.43	1.40										
Na_2O	3.09	3.12	3.01	3.14	2.04	2.05										
K_2O	2.15	1.83	1.88	2.07	3.23	3.28										
P_2O_5	0.47	0.48	0.39	0.45	0.14	0.16										
LOI	1.37	1.18	1.26	1.55	1.56	1.56										
Total	99.88	99.48	99.54	99.81	99.51	99.76										
Mg#	39.0	40.9	41.0	40.0												
ASI	0.88	0.86	0.84	0.87												
ANCK	0.84	0.82	0.81	0.83												
Na+K/Al	0.66	0.65	0.63	0.65												
K_2O/Na_2O	0.69	0.59	0.62	0.66												
Sc (ppm)	24	19.5	16.8	22.5			11.8	13	33.0	33	31.8	32	44.5	44	31.2	31
V	149.9	98.29	82.9	183.3			117.6	120	414.1	416	316.6	317	326.0	313	156.5	148
Cr	4	4	4	4			17.0	17	17.0	18	280.0	280	384.0	382	282.5	285
Co	33.9	35	28.8	33.1			15.1	16	36.4	37	43.6	45	52.2	51.4	55.9	54.7
Ni	20	16	16	18			17.0	19	11.0	13	112.6	119	165.8	166	250.5	247
Cu	45.1	41.0	70.4	40.1			49.6	53	18.7	19	127.8	127	120.0	126	96.9	96
Zn	88.9	139.5	93.2	99.4			75.8	86	137.4	127	110.9	103	59.7	71	51.0	66
Ga	20.9	20	17.3	20.2			20.2	20	22.6	23	22.0	21.7	16.1	16	14.3	15
Rb	70	60	56	74			68.0	68.6	49.0	48	9.6	9.8	0.2	0.24	3.8	4.5
Sr	173	156	135	156			648.0	658	345.5	346	403.0	389	116.0	110	151.5	145
Y	44.1	49.2	42.1	46.1			19.5	20	36.5	37	26.8	26	16.4	16	18.1	18
Zr	307	341	293	320			229.5	230	187.5	188	173.5	172	16.0	14	40.0	41
Nb	22.9	25.9	21.5	24.8			13.9	15	12.3	12.5	18.3	18	0.5	0.5	1.5	2
Cs	2.4	1.3	1.6	2.7			1.1	1.16	1.1	1.1	0.1	0.1	0.0	0.007	0.2	0.3
Ba	405	402	370	359			1129.0	1140	697.5	683	154.5	130	8.0	7.2	124.5	118
La	29.3	31.6	30.2	30.6			32.1	38	24.9	25	15.3	15	0.6	0.675	3.7	3.53
Ce	72.1	78.3	64.8	73.7			67.7	68	53.0	53	38.4	38	2.2	2.11	9.4	8.19
Pr	9.15	10.08	8.31	9.5			8.1	8.3	6.9	6.8	5.5	5.29	0.4	0.35	1.1	1.1
Nd	37.3	41.5	33.8	38.6			29.7	30	28.7	28	24.6	25	2.4	2.37	5.0	4.86
Sm	8.72	9.96	8.11	9.1			5.5	5.7	6.7	6.7	6.3	6.2	1.1	1.12	1.5	1.4
Eu	2.354	2.51	2.108	2.275			1.6	1.54	2.0	2	2.1	2.07	0.5	0.528	0.6	0.6
Gd	8.86	10.24	8.47	9.22			4.5	4.69	6.8	6.8	6.3	6.3	2.0	1.83	2.2	2
Tb	1.37	1.60	1.35	1.44			0.6	0.64	1.1	1.07	1.0	0.9	0.4	0.36	0.4	0.39
Dy	8.11	9.59	8.15	8.57			3.4	3.6	6.4	6.41	5.4	5.31	2.6	2.51	2.8	2.75
Ho	1.72	2.01	1.70	1.81			0.7	0.71	1.3	1.33	1.0	1.04	0.6	0.55	0.7	0.65
Er	4.58	5.34	4.5	4.82			1.8	1.79	3.6	3.66	2.5	2.54	1.7	1.66	1.9	1.9
Tm	0.67	0.76	0.65	0.71			0.3	0.26	0.5	0.54	0.3	0.34	0.3	0.25	0.3	0.3
Yb	4.12	4.64	4.04	4.38			1.6	1.6	3.4	3.5	2.0	2	1.7	1.65	2.0	1.97
Lu	0.59	0.65	0.57	0.63			0.2	0.25	0.5	0.51	0.3	0.28	0.3	0.255	0.3	0.309
Hf	7.86	8.64	7.48	8.06			5.1	5.08	4.8	4.8	4.4	4.1	0.6	0.4	1.0	1.05
Ta	1.59	1.77	1.47	1.68			0.9	0.89	0.8	0.81	1.2	1.4	0.0	0.06	0.1	0.098
Th	8.01	9.01	7.80	8.27			6.2	6.1	6.1	6.2	1.2	1.2	0.0	0.033	0.3	0.22
U	1.38	1.96	1.68	1.55			1.9	1.88	1.7	1.69	0.4	0.42	0	0.01	0.1	0.05
La/Yb$_N$	5.1	4.9	5.4	5.0												
Eu/Eu*	0.81	0.75	0.77	0.75												

[a]Mg# = [Mg^{2+}/(Mg^{2+} + Fe_2^{2+})]*100. N = normalized to chrondite values of *Sun and McDonough* [1989]. m.v., measured value; r.v., recommended value.

composition is similar to sample MCK1 (Table 1). The same modeling parameters for sample C2-59 are used to model sample 13. Alkali feldspar ($An_3Ab_{50}Or_{47}$) crystallizes first at 990°C followed by Ti-rich spinel (i.e., titanomagnetite) at 950°C and quartz at 910°C. During the later stages (i.e., <910°C) of crystallization, plagioclase (An_{28}), fayalite (870°C) and ilmenite crystallize (860°C).
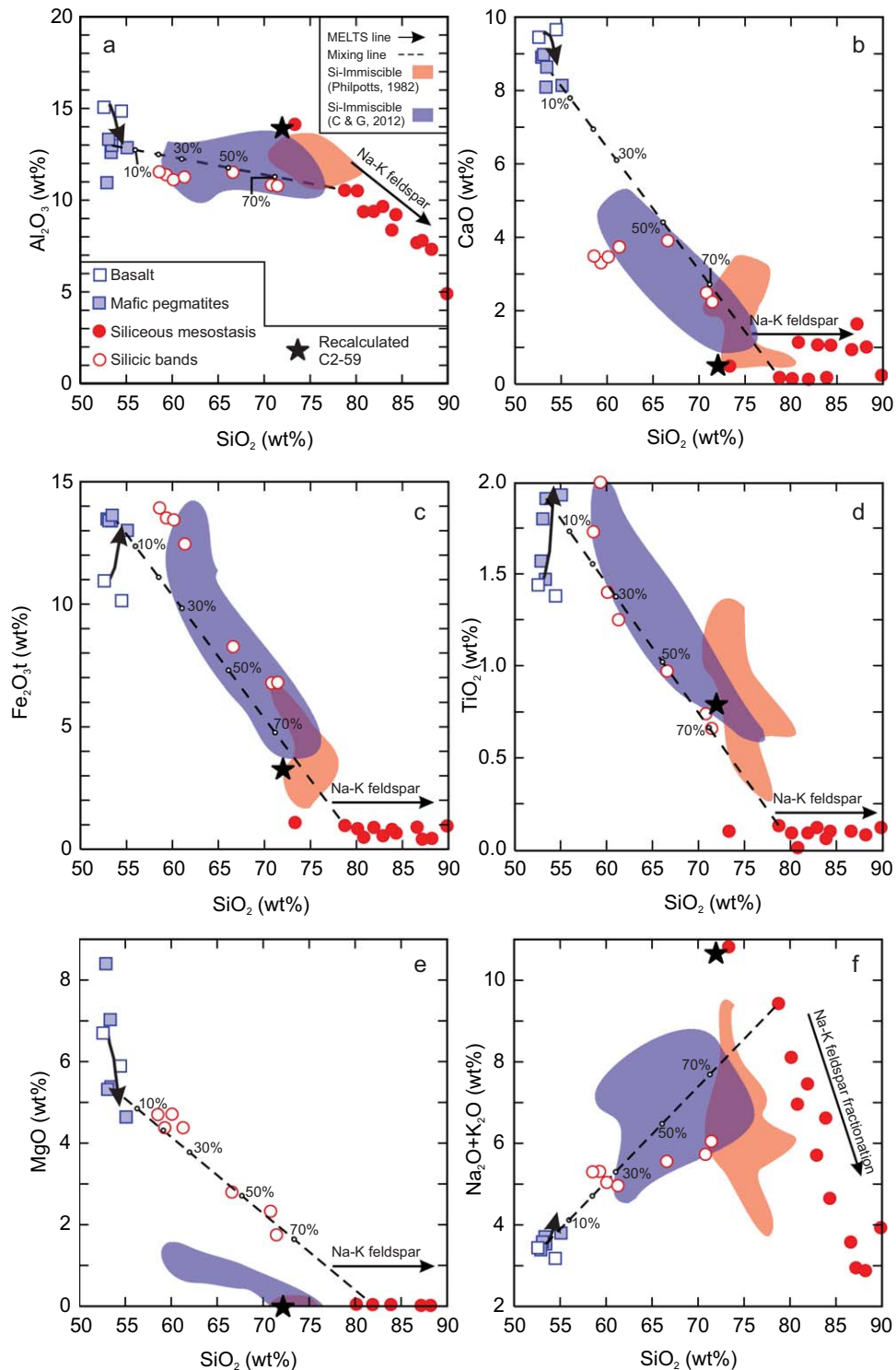
Figure 2. Harker diagrams showing the chemical variation of the granophyres, mesostasis, mafic pegmatites, and basalts. The dashed line represents a best-fit mixing line between the siliceous mesostasis and the mafic pegmatites. The solid arrow is the MELTS modeling line from the basalt (MCK1) to the mafic pegmatite. The red field is the range of Si-rich immiscible liquids from *Philpotts* [1982] whereas the blue field is the range if Si-rich immiscible liquids from *Charlier and Grove* [2012]. Additional data of the granophyres bands, pegmatites, and basalts are from *Geenough and Dostal* [1992a]. All data including MELTS models are plotted as anhydrous.

6. Discussion

6.1. Magmatic Conditions for Silicate-Liquid Immiscibility at McKay Head

[21] The magmatic conditions for two silicate-liquid immiscibility include the following criteria: (1) ideally low pressure (∼0.3 kbar) so that plagioclase dominates early crystallization to enrich the residual liquid in iron, (2) temperatures between 1000°C and 1285°C although there are few experimental constraints at >1200°C [*Philpotts*, 1972, 1978; *Hess et al.*, 1975; *Visser and van Groos*, 1979; *Philpotts and Doyle*, 1980; *Hurai et al.*, 1998; *Charlier and Grove*, 2012], and (3) a relatively dry, bulk magmatic system which ideally but not necessarily is enriched in TiO_2, P_2O_5, and alkalis [*Yoder*, 1973; *Freestone*, 1978; *Philpotts*, 1979, 1982; *Charlier and Grove*, 2012].

[22] The magmatic conditions of the basaltic rocks at McKay Head indicate that they were suitable for immiscibility. First, the reported maximum surface thickness of the North Mountain basalt is ∼400 m which thins to ∼275 m near McKay Head. The fact that the basalts at McKay Head erupted means the depth of emplacement and crystallization was at or very near atmospheric pressure. Second, the paucity of hydrous minerals such as amphibole or mica in the North Mountain basalts and the presence of quartz and alkali (sanidine) feldspar in the granophyres suggests magmatic water content was probably similar to typical continental tholeiitic (i.e., $H_2O = 0.4$ wt% to 0.6 wt%) magmas during eruption [*Danyushevsky*, 2001]. However, recent experimental work suggests water may play a role in stabilizing the liquid-phase separation in some water-rich silicate magma systems at 200 MPa [*Lester et al.*, 2013]. The estimated eruption temperature for crystal free lava equal to the basalts at McKay Head calculated using pHMELTS is no higher than 1170°C, assuming bulk water content of 0.5 wt%. The calculated crystal-free temperature is above the temperature required for immiscibility at anhydrous and low pressures conditions but there is insufficient experimental work to rule out the possibility that silicate immiscibility cannot occur at higher temperatures [*Charlier and Grove*, 2012].

[23] Parental magmas do not "unmix" immediately upon eruption but rather they undergo an early stage of crystallization or crystal fractionation which drives the residual liquid composition toward conditions of immiscibility [*Freestone*, 1978]. There is evidence for early fractional crystallization

within the McKay Head flow. Figure 2 shows Harker diagrams of the basalts, pegmatites, silicic bands and mesostases. The Harker diagrams clearly show that Fe_2O_3, TiO_2, and P_2O_5 increase whereas Al_2O_3, MgO, and CaO decrease with increasing SiO_2. The alkalis (i.e., Na_2O and K_2O) increase modestly with increasing SiO_2. MELTS modeling using the basalt composition from McKay Head (i.e., sample MCK1 from *Greenough and Dostal* [1992a]) confirms that fractionation of clinopyroxene and plagioclase (An_{72-65}) occurred before liquid compositions reached that of the pegmatites. Plagioclase compositions reported by *Dostal and Greenough* [1992] from the North Mountain basalt are very similar to the modeled crystal compositions (i.e., An_{72}). The fact that plagioclase fractionated relatively early in the system suggests that water content was not particularly high because water suppresses the crystallization of plagioclase in favor of mafic silicate minerals [*Sisson and Grove*, 1993; *Botcharnikov et al.*, 2008]. When the residual liquid composition of the MELTS model reaches that of the pegmatite (i.e., ∼30% solid, 70% liquid), the temperature is still relatively high at 1150–1140°C but perhaps most importantly the remaining liquid is relatively enriched in Fe, Ti, P, and alkalis (Figures 2 and 3).

[24] Experiments show that the field of immiscibility will expand with increasing oxygen fugacity [*Philpotts and Doyle*, 1983; *Naslund*, 1983; *Vicenzi et al.*, 1994]. The relative oxidation state of a magma will govern the timing of crystallization and composition of Fe-Ti oxides within the system [*Buddington and Lindsley*, 1964; *Toplis and Carroll*, 1995]. If the relative oxidation state of a mafic magma is higher (e.g., NNO buffer) during the early stages of crystallization then magnetite or titanomagnetite will crystallize early and prevent subsequent Fe-Ti-P enrichment and therefore diminishes the likelihood that immiscibility would occur. We estimated the relative oxidation state of the pegmatite and the granophyric layers using magnetite-ilmenite pairs [*Anderson et al.*, 1993]. Ilmenite and magnetite compositions from the pegmatite reported by *Greenough and Dostal* [1992b] indicate that they crystallized near the FMQ buffer (i.e., $\Delta FMQ + 0.8$). In comparison the ilmenite and magnetite pairs within sample MH12-002 have the largest range from ΔFMQ −0.4 to +1.7. Additionally, the calculated fO_2 for the basalts at McKay Head using the method of *Kress and Carmichael* [1991], assuming temperatures of 1150°C at surface pressure, gave values at the FMQ buffer. The results suggest that the
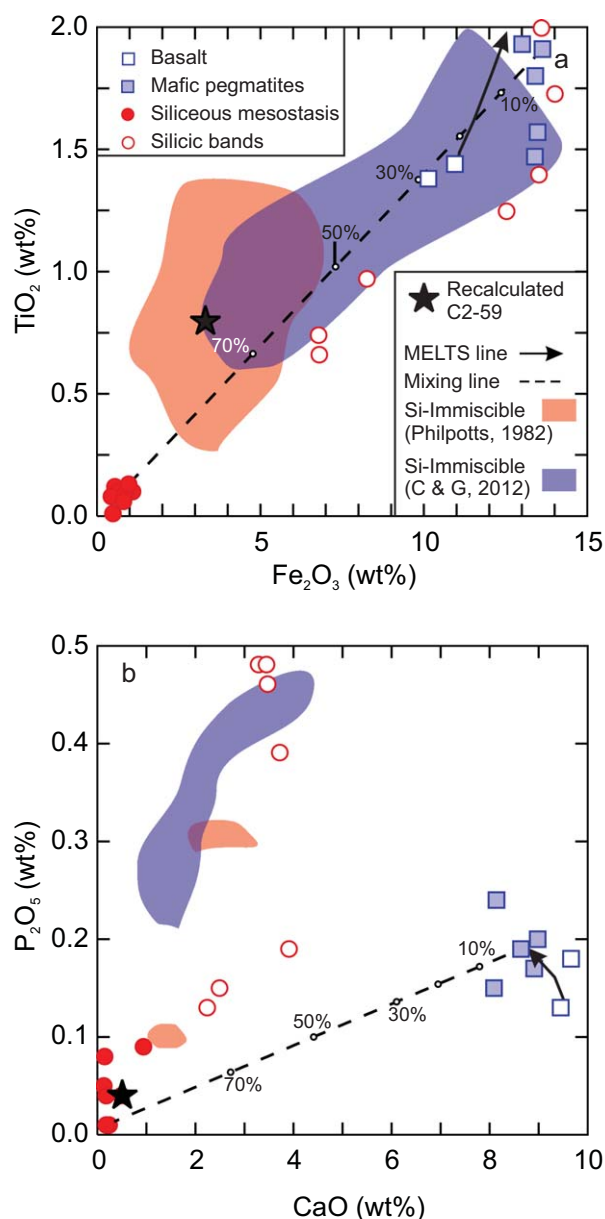
Figure 3. (a) TiO_2 wt% versus Fe_2O_3t wt% and (b) P_2O_5 wt% versus CaO wt% of the rocks and mesostasis from McKay Head. The dashed line represents a best-fit mixing line between the siliceous mesostasis and the mafic pegmatites. The solid arrow is the MELTS modeling line from the basalt (MCK1) to the mafic pegmatite. The red field is the range of Si-rich immiscible liquids from *Philpotts* [1982] whereas the blue field is the range if Si-rich immiscible liquids from *Charlier and Grove* [2012]. Additional data of the silicic bands, pegmatites, and basalts are from *Geenough and Dostal* [1992a]. All data including MELTS models are plotted as anhydrous.

relative oxidation state of the parental magma was not extremely oxidizing as it is within the range (i.e., FMQ ± 2) of the mantle but it is interesting that it appears to have increased from ΔFMQ

+0.8 in the pegmatite to ΔFMQ +1.7 in the granophyric layers which is more favorable for two silicate-liquid immiscibility [*Arculus*, 1985; *Kasting et al.*, 1993; *Frost and McCammon*, 2008]. Therefore, we conclude that the magmatic conditions at McKay Head were suitable for silicate-liquid immiscibility to occur.

6.2. Origin of the Granophyric Layers

[25] The granophyres are composed of two distinct components, minerals and siliceous mesostasis. It is highly unlikely that that the granophyres represent a distinct magma or postmagmatic feature largely due to their location within the basalt flow and the fact that the Sr and Nd isotopes (i.e., $εNd_{(T)} = −1.5$ to $−1.7$; $I_{Sr} = 0.70613$ to 0.70627) overlap completely with the North Mountain basalts and CAMP basalts [*Jones and Mossman*, 1988; *Greenough and Dostal*, 1992b; *Pe-Piper et al.*, 1992; *Dostal and Durning*, 1998; *Murphy et al.*, 2011]. The major issue is whether the minerals and mesostases are from one silicate liquid or two.

[26] Previous studies by *Greenough and Dostal* [1992b] and *Kontak and Dostal* [2010] suggested that the granophyric rocks formed by fractional crystallization and subsequent filter pressing to concentrate a residual silicic liquid to form the layers and pipes observed in the upper flow. The fractional-filtering interpretation is consistent with the bulk compositions of the granophyres because Si-rich silicate-liquid immiscible compositions reported by *Philpotts* [1982] and *Charlier and Grove* [2012] are extremely depleted in MgO (Figure 2). The granophyres have between 1.7 wt% and 5.0 wt% MgO whereas siliceous immiscible liquid compositions have very low MgO (i.e., <1.4 wt%). The highest reported MgO content by *Charlier and Grove* [2012] is 1.4 wt% in a sample (i.e., SI-13) with 60.4 wt% SiO_2. The contradiction in MgO content implies that the bulk rock composition of the granophyric layers cannot represent an immiscible silicate liquid unto itself. However, the composition of the granoiphyres fall between the mafic pegmatites reported at McKay Head and the mesostases indicating a mixing relationship. The best fit mixing line shown in Figures 2 and 3 indicates that the granophyres represent between 10–70% silicic mesostasis and 90–30% minerals (i.e., augite, ferroaugite, stilpnomelane, apatite, plagioclase, ilmenite, magnetite, quartz, and alkali feldspar).

[27] The silicic mesostases analyzed in this paper bear some resemblance (i.e., Ca, Na, K) to reported

immiscible siliceous liquids but overall there are some differences (i.e., Ti, Fe). The mesostases tend to have high to very high Si (i.e., >75 wt%) and very low Fe (i.e., Fe_2O_3 <2 wt%) and Ti (i.e., TiO_2 <0.2 wt%) whereas the Si-rich immiscible compositions reported by *Philpotts* [1982] and *Charlier and Grove* [2012] tend to have lower Si (i.e., SiO_2 <75 wt.%) and higher Fe (i.e., Fe_2O_3 >2 wt%) and Ti (i.e., TiO_2 >0.25 wt%). Sample C2-59 has the lowest SiO_2 content and is most similar to the data reported by *Philpotts* [1982] but it is deficient in Fe and Ti. The compositional differences between the mesostases and the Si-rich composition may simply be due to crystallization of Fe-Ti oxide minerals, quartz and sanidine. Therefore, it is possible that the silicic mesostasis represent Si-rich immiscible liquids that originally formed at lower SiO_2 contents (i.e., $SiO_2 \approx 70$ wt%) and subsequently crystallized other minerals, such as alkali feldspar. The effects of alkali feldspar crystallization on the mesostases are seen in Figure 2. If we assume the Fe and Ti contents of C2-59 were higher or at least equal to sample 13 in Table 1 and back calculate the composition then the original liquid falls close to the immiscibility field (Figures 2 and 3).

[28] If the immiscible silicic liquid equals a composition similar to sample C2-59, the first mineral to crystallize, based on MELTS models, would be sanidine ($An_1Ab_{47}Or_{52}$) at 1070°C followed by quartz at 930°C and titanomagnetite at 910°C. In comparison, if the silicic immiscible composition 13 (Table 1) from *Philpotts* [1982] is used, the first mineral to crystallize is sanidine ($An_3Ab_{50}Or_{47}$) at 990°C followed by titanomagnetite at 950°C and quartz at 910°C. The fact that quartz and more-potassic alkali feldspar ($An_1Ab_{33}Or_{66}$) are found in contact with the silicic mesostasis in the granophyre suggests that they may have crystallized from a liquid similar to the original mesostasis liquid which has further differentiated to even higher silica values (i.e., >80 wt%) after its initial formation. The observed alkali feldspar compositions overlap completely with the modeled compositions thereby corroborating the MELTS models. In addition, minerals analyzed in the granophyre, such as plagioclase and ferroaugite, would not crystallize from a magma equal to a Si-rich immiscible liquid. In other words, there would be no plagioclase or ferroaugite thus some of the silicic (i.e., lower SiO_2 analysis) mesostases are probably closer to actual immiscible silicic liquids whereas other mesostases (i.e., SiO_2 >75 wt%) represent evolved immiscible silicic compositions after crystallization of alkali feldspar and quartz.

[29] The presence of ferrorichterite and stilpnomelane within the granophyre may be supportive of silicate-liquid immiscible separation. Stilpnomelane is commonly found within metamorphosed banded iron formations but not basaltic rocks [*Miyano and Klein*, 1989]. It is very likely that the stilpnomelane formed when the residual basalt liquid was becoming Fe-rich. Iron-rich immiscible silicate-liquids are relatively depleted in Al (i.e., 3.1 wt% in sample 13 from *Philpotts* [1982]) and will require a host mineral thus stilpnomelane and possibly ferroaugite may be indicator minerals for the formation of Fe-rich immiscible silicate-liquids. In contrast ferrorichterite is a common mineral within metaluminous to peralkaline silicic rocks and probably crystallized from the Si-rich immiscible liquid [*Shellnutt and Iizuka*, 2011].

6.3. Model of Formation

[30] The mesostases appear to result from silicate-liquid immiscibility. The estimates for the magmatic conditions (i.e., pressure, temperature, relative oxidation state) and the bulk composition of the mesostases (i.e., sample C2-59) are consistent with petrological modeling of silicate-liquid immiscibility [*Philpotts*, 1982; *Charlier and Grove*, 2012]. We propose a fractionation-immiscible model to explain the features observed within the basalt pile at McKay Head.

[31] Basalt equal or similar to the composition MCK1 erupted (Figure 4a) and began to crystallize augite and plagioclase (An_{72}) (Figure 4b). The relative $\times O_2$ condition was at or near the FMQ buffer and the eruptive temperature was ≤1150°C. After augite and plagioclase crystallize (i.e., ~30%), the residual liquid (i.e., ~70%) composition is relatively enriched in Fe-Ti-P and meets the conditions suitable for silicate-liquid immiscibility (Figure 4b). The Fe-rich immiscible liquid end-member, although not observed in this study, forms and crystallizes ferroaugite, plagioclase, stilpnomelane, and Fe-Ti oxide minerals whereas the Si-rich immiscible end-member has a bulk composition similar to mesostasis sample C2-59 but with a higher bulk Fe_2O_3t and TiO_2 composition before subsequent crystallization of sanidine, Fe-Ti oxide minerals and quartz ± ferrorichterite (Figure 4c). The Fe-rich immiscible end-member is not observed because it is intermingled with parts of the mafic pegmatite and it appears Fe-rich mesostasis were not preserved. The granophyric layers are therefore mixtures of immiscible siliceous liquid and minerals derived from previous crystallization and postimmiscible separation
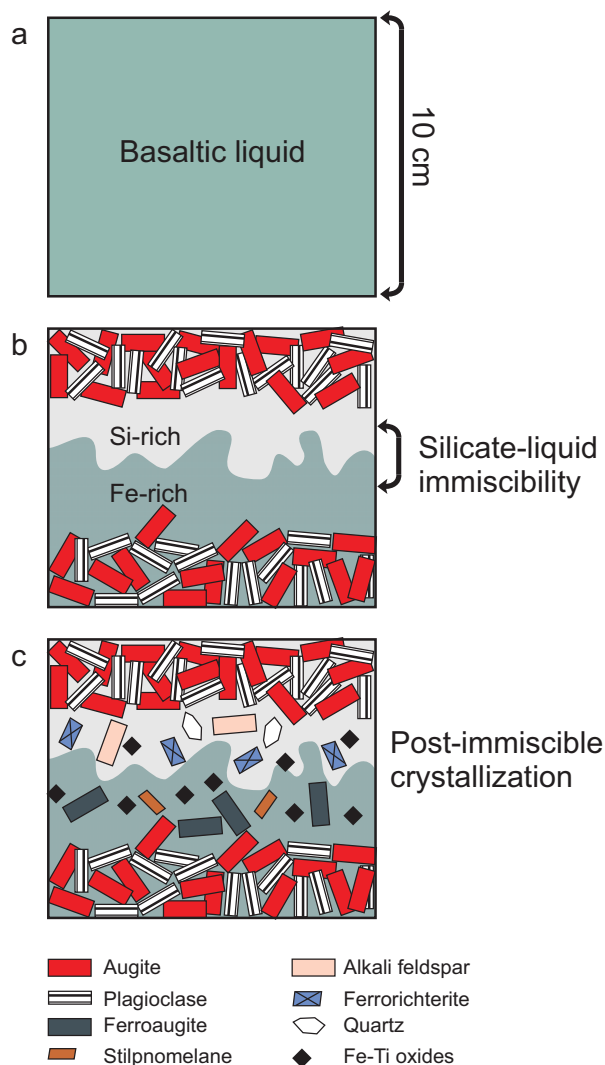
Figure 4. Conceptual model of silicate-liquid immiscibility within the basalts from McKay Head. (a) A basaltic liquid erupts and (b) begins to crystallize clinopyroxene and plagioclase. After sufficient crystallization (i.e., ~30%) the residual liquid becomes Fe-Ti-P-rich and separates into two silicate liquids. (b) The two liquids then start to crystallize within their respective domains. (c) The Fe-rich silicate-liquid crystallizes ferroaugite, Fe-Ti oxides, and stilpnomalene whereas the Si-rich liquid crystallizes alkali feldspar, quartz, and Fe-Ti oxides ± ferrorichterite.

crystallization. In some cases the granophyre layers may be up to 70% immiscible silicic material. The separation of the two silicate-liquids occurs within a small framework that was <10 cm thick and can represent 10–50% of an individual pegmatite layer. We conservatively estimate that the total volume of silicic material derived by immiscibility at McKay Head to be in the range of 300–400 m³ assuming an average height of the granophyre layers (i.e., 8–9 layers) to be 0.04 m and using the dimensions of the outcrop, length of

~100 m and width of ~10 m [*Greenough and Dostal*, 1992a, 1992b]. The total volume of immiscible liquids is a small fraction (i.e., ~1%) of the entire exposure (i.e., ~3.4 × 10⁴ m³) at McKay Head however the identification of "greater-than-micron-scale" evidence of silicate-liquid immiscibility suggests that, given a mechanism to concentrate the individual silicate-liquids, it may be a viable large-scale volcanic or plutonic process.

7. Conclusions

[32] The silicic mesostases within the basalt flows at McKay Head were formed by immiscible segregation from a parental magma which resembled continental flood basalt from the northern Central Atlantic Magmatic Province. The mafic pegmatite within the basaltic flows is composed of crystals which formed prior to immiscibility. The early crystallization of augite and plagioclase from the parental magma drove the residual liquid composition toward higher Fe-Ti-P concentrations. The "granophyric layers" within the basalt flows are actually mixtures of minerals (i.e., ilmenite, magnetite, ferroaugite, plagioclase, stilpnomelane, apatite) from the Fe-rich immiscible liquid and minerals (i.e., sanidine, quartz, ferrorichterite) and silicic mesostasis from the Si-rich immiscible liquid. The identification of silicate immiscibility at observable scales greater than micron level suggests that it could be a common feature of some continental flood basalts. However, the viability of silicate-liquid immiscibility as a large-scale process (i.e., meter-scale) capable of forming bimodal mafic-felsic volcanic and plutonic suites needs to be constrained further.

Acknowledgments

References

Anderson, D. J., D. H. Lindsley, and P. M. Davidson (1993), QUILF: A Pascal program to assess equilibria among

Fe-Mg-Mn oxides, pyroxenes, olivine, and quartz, *Comput. Geosci.*, *19*, 1333–1350.

Arculus, R. A. (1985), Oxidation status of the mantle: Past and present, *Annu. Rev. Earth Planet. Sci.*, *13*, 75–95.

Botcharnikov, R. E., R. R. Almeev, J. Koepke, and F. Holtz (2008), Phase relations and liquid lines of descent in hydrous ferrobasalt—Implications for the Skaergaard intrusion and Columbia River basalts, *J. Petrol.*, *49*, 1687–1727.

Bowen, N. L. (1916), Discussion of ''Magmatic differentiation in effusive rocks,'' *Trans. AIME*, *54*, 455–457.

Buddington, A. F., and D. H. Lindsley (1964), Iron-titanium oxide minerals and synthetic equivalents, *J. Petrol.*, *5*, 310–357.

Charlier, B., O. Namur, M. J. Toplis, P. Schiano, N. Cluzel, M. D. Higgins, and J. Vander Auwera (2011), Large-scale silicate immiscibility during differentiation of tholeiitic basalt to granite and the origin of the Daly gap, *Geology*, *39*, 907–910.

Charlier, D., and T. L. Grove (2012), Experiments on liquid immiscibility along tholeiitic liquid lines of descent, *Contrib. Mineral. Petrol.*, *164*, 27–44.

Danyushevsky, L. V. (2001), The effect of small amounts of H_2O on crystallization of mid-ocean ridge and back-arc basin magmas, *J. Volcanol. Geotherm. Res.*, *110*, 265–280.

Dixon, S., and M. J. Rutherford (1979), Plagiogranites as late-stage immiscible liquids in ophiolite and mid-ocean ridge suites: An experimental study, *Earth Planet. Sci. Lett.*, *45*, 45–60.

Dostal, J., and C. Dupuy (1984), Geochemistry of the North Mountain basalts (Nova Scotia, Canada), *Chem. Geol.*, *45*, 245–261.

Dostal, J., and M. Durning (1998), Geochemical constraints on the origin and evolution of early Mesozoic dikes in Atlantic Canada, *Eur. J. Min.*, *10*, 79–93.

Dostal, J., and J. D. Greenough (1992), Geochemistry and petrogenesis of the early Mesozoic North Mountain basalts of Nova Scotia, Canada, in *Eastern North America Mesozoic Magmatism*, vol. *268*, edited by J. H. Puffer and P. C. Ragland, pp. 149–159, Geol. Soc. of Am., Boulder, Colorado.

Duchesne, J. C. (1999), Fe-Ti deposits in Rogaland anorthosites (South Norway): Geochemical characteristics and problems of interpretation, *Miner. Deposita*, *34*, 182–198.

Dupuy, C., and J. Dostal (1984), Trace element geochemistry of some continental tholeiites, *Earth Planet. Sci. Lett.*, *67*, 61–69.

Eby, G. N. (1980), Mount Johnson, Quebec—An example of silicate-liquid immiscibility?, *Geology*, *7*, 491–494.

Ferreira, V. P., A. N. Sial, and J. A. Whitney (1994), Large scale silicate liquid immiscibility: A possible example from northeastern Brazil, *Lithos*, *33*, 285–302.

Freestone, I. C. (1978), Liquid immiscibility in alkali-rich magmas, *Chem. Geol.*, *23*, 115–123.

Frost, D. J., and C. A. McCammon (2008), The redox state of the Earth's mantle, *Annu. Rev. Earth Planet. Sci.*, *36*, 389–420.

Ghiorso, M. S., and R. O. Sack (1995), Chemical mass transfer in magmatic processes IV. A revised and internally consistent thermodynamic model for the interpolation and extrapolation of liquid-solid equilibria in magmatic systems at elevated temperatures and pressures, *Contrib. Mineral. Petrol.*, *119*, 197–212.

Greenough, J. D., and J. Dostal (1992a), Layered rhyolite bands in a thick North Mountain basalt flow: The products of silicate liquid immiscibility, *Mineral. Mag.*, *56*, 309–318.

Greenough, J. D., and J. Dostal (1992b), Cooling history and differentiation of a thick North Mountain basalt flow (Nova Scotia, Canada), *Bull. Volcanol.*, *55*, 63–73.

Greenough, J. D., and V. S. Papezik (1987), Note on the petrology of North Mountain basalt from the wildcat oil well Mobil Gulf Chinampas N-37, Bay of Fundy, Canada, *Can. J. Earth Sci.*, *24*, 1255–1260.

Hess, P. C., M. J. Rutherford, R. N. Guillemette, F. J. Ryerson, and H. A. Tuchfeld (1975), Residual products of fractional crystallization of lunar magmas: An experimental study, Lunar Science Conference, 6th, Houston, Tex., March 17–21, 1975, Proceedings. Volume 1. (A78-46603 21-91) New York, Pergamon Press, Inc., 1975, p. 895-909.

Hodych, J. P., and G. R. Dunning (1992), Did the Manicouagan impact trigger end-of-Triassic mass extinction?, *Geology*, *20*, 51–54.

Hurai, V., K. Simon, U. Wiechert, J. Hoefs, P. Koneny, M. Huraiova, J. Pironon, and J. Lipka (1998), Immiscible separation of metalliferous Fe/Ti-oxide melts from fractionating alkali basalt: $P\text{-}T\text{-}f_{O_2}$ conditions and two liquid elemental partitioning, *Contrib. Mineral. Petrol.*, *133*, 12–29.

Jahn, B.-M. (2004), The central Asian orogenic belt and growth of the continental crust in the Phanerozoic, in *Aspects of the Tectonic Evolution of China*, vol. *226*, edited by J. Malpas et al., pp. 73–100, Geol. Soc. London Spec. Publ.

Jakobsen, J. K., I. V. Veksler, C. Tegner, and C. K. Brooks (2005), Immiscible iron- and silica-rich melts in basalt Petrogenesis documented in the Skaergaard intrusion, *Geology*, *33*, 885–888.

Jones, L. M., and D. J. Mossman (1988), The isotopic composition of strontium and the source of the Early Jurassic North Mountain basalts, Nova Scotia, *Can. J. Earth Sci.*, *25*, 942–944.

Jourdan, F., A. Marzoli, H. Bertrand, S. Cirilli, L. H. Tanner, D. J. Kontak, G. McHone, P. R. Renne, and G. Bellieni (2009), $^{40}Ar/^{39}Ar$ ages of CAMP in North America: Implications for the Triassic–Jurassic boundary and the ^{40}K decay constant bias, *Lithos*, *110*, 167–180.

Kasting, J. F., D. H. Eggler, and S. P. Raeburn (1993), Mantle redox evolution and the oxidation state of the Archean atmosphere, *J. Geol.*, *101*, 245–257.

Kolker, A. (1982), Mineralogy and geochemistry of Fe-Ti oxide and apatite (nelsonite) deposits and evaluation of the liquid immiscibility hypothesis, *Econ. Geol.*, *77*, 1146–1158.

Kontak, D. J. (2008), On the edge of CAMP: Geology and volcanology of the Jurassic North Mountain basalt, Nova Scotia, *Lithos, 101*, 39–66.

Kontak, D. J., and D. A. Archibald (2003), $^{40}Ar/^{39}Ar$ age dating of the Jurassic North Mountain Basalt, southern Nova Scotia, *Atl. Geol.*, *39*, 47–54.

Kontak, D. J., and J. Dostal (2010), The late-stage crystallization history of the Jurassic North Mountain basalt, Nova Scotia, Canada. II. Nature and origin of segregation pipes, *Can. Mineral.*, *48*, 1533–1568.

Kontak, D. J., M. Y. De Wolfe-De Young, and J. Dostal (2002), Late stage crystallization history of the Jurassic North Mountain basalt, Nova Scotia, Canada. I. Textural and chemical evidence for pervasive development of silicate-liquid immiscibility, *Can. Mineral.*, *40*, 1287–1311.

Kontak, D. J., J. Dostal, and J. D. Greenough (2005), *Geology and Volcanology of the Jurassic North Mountain Basalt, Southern Nova Scotia*, Geol. Assoc. of Canada-Mineral.

Assoc. of Canada Annu. Meet., Field Trip B3, 131 pp., Atlantic Geoscience Society, Wolfville, Nova Scotia.

Kress, V. C., and I. S. E. Carmichael (1991), The compressibility of silicate liquids containing Fe_2O_3 and the effect of composition, temperature, oxygen fugacity and pressure on their redox states, *Contrib. Mineral. Petrol.*, *108*, 82–92.

Lester, G. W., A. H. Clark, Kyser, T. K., and H. R. Naslund (2013), Experimental on liquid immiscibility in silicate melts with H_2O, P, S, F and Cl: Implications for natural magmas. *Contrib. Mineral. Petrol.*, *166*, 329–349.

McBirney, A. R. (1975), Differentiation of the Skaergaard Intrusion, *Nature*, *253*, 691–694.

McHone, J. G., D. L. Anderson, E. K. Beutel, and Y. A. Fialko (2005), Giant dikes, rifts, flood basalts, and plate tectonics: A contention of mantle models, in *Plates, Plumes, and Paradigms*, vol. *388*, edited by G. R. Foulger et al., pp. 401–420, Geol. Soc. of Am., Boulder, Colorado

Miyano, T., and C. Klein (1989), Phase equilibria in the system K_2O-FeO-MgO-Al_2O_3-SiO_2-H_2O-CO_2 and the stability limit of stilpnomelane in metamorphosed Precambrian iron-formations, *Contrib. Mineral. Petrol.*, *102*, 478–491.

Murphy, J. B., and J. Dostal (2007), Continental mafic magmatism of different ages in the same terrane: Constraints on the evolution of an enriched mantle source, *Geology*, *35*, 335–338.

Murphy, J. B., J. Dostal, G. Gutierrez-Alonso, and J. D. Keppie (2011), Early Jurassic magmatism on the northern margin of CAMP: Derivation from a Proterozoic subcontinental lithospheric mantle, *Lithos*, *123*, 158–164.

Namur, O., B. Charlier, M. J. Toplis, M. D. Higgins, V. Hounsell, J.-P. Liegeois, and J. Vander Auwera (2011), Differentiation of tholeiitic basalt to A-type granite in the Sept Iles layered intrusion, Canada, *J. Petrol.*, *52*, 487–539.

Naslund, H. R. (1983), The effect of oxygen fugacity on liquid immiscibility in iron-bearing silicate melts, *Am. J. Sci.*, *283*, 1034–1059.

Olsen, P. E. (1997), Stratigraphic record of the early Mesozoic breakup of Pangea in the Laurasia–Gondwana rift system, *Annu. Rev. Earth Planet. Sci.*, *25*, 337–401.

Olsen, P. E., N. H. Shubin, and M. H. Anders (1987), New early Jurassic tetrapod assemblages constrain Triassic-Jurassic tetrapod extinction event, *Science*, *237*, 1025–1029.

Olsen, P. E., R. W. Schlische, and M. S. Fedosh (1998), 580 ka duration of the Early Jurassic flood basalt event in eastern North America estimated using Milankovitch cyclostratigraphy, in *The Continental Jurassic, Mus. of North Ariz. Bull. 60*, edited by M. Morales, pp. 11–22, Flagstaff, Arizona.

Papezik, V. S., J. D. Greenough, J. A. Colwell, and T. J. Mallinson (1988), North Mountain basalt from Digby, Nova Scotia: Models for a fissure eruption from stratigraphy and petrochemistry, *Can. J. Earth Sci.*, *24*, 74–83.

Pe-Piper, G., L. F. Jansa, and R. S. Lambert (1992), Early Mesozoic magmatism on the eastern Canadian margin: Petrogenetic and tectonic significance, in *Eastern North America Mesozoic Magmatism*, vol. *268*, edited by J. H. Puffer and P. C. Ragland, pp. 13–36, Geol. Soc. of Am., Boulder, Colorado.

Philpotts, A. R. (1967), Origin of certain iron-titanium oxide and apatite rocks, *Econ. Geol.*, *62*, 303–315.

Philpotts, A. R. (1972), Density, surface tension and viscosity of the immiscible phase in a basic, alkaline magma, *Lithos*, *5*, 1–18.

Philpotts, A. R. (1976), Silicate liquid immiscibility: Its probable extent and petrogenetic significance, *Am. J. Sci.*, *276*, 1147–1177.

Philpotts, A. R. (1978), Textural evidence for liquid immiscibility in tholeiites, *Mineral. Mag.*, *42*, 417–425.

Philpotts, A. R. (1979), Silicate liquid immiscibility in tholeiitic basalts, *J. Petrol.*, *20*, 99–118.

Philpotts, A. R. (1982), Compositions of immiscible liquids in volcanic rocks, *Contrib. Mineral. Petrol.*, *80*, 201–218.

Philpotts, A. R., and C. D. Doyle (1980), Immiscibility in tholeiites: a discussion, *Mineral. Mag.*, *43*, 939–940.

Philpotts, A. R., and C. D. Doyle (1983), Effect of magma oxidation state on the extent of silicate immiscibility in a tholeiitic basalt, *Am. J. Sci.*, *283*, 967–986.

Powers, S. (1916), The Acadian Triassic, *J. Geol.*, *24*, 1–26.

Powers, S., and A. C. Lane (1916), Magmatic differentiation in effusive rocks, *Trans. AIME*, *54*, 442–455.

Roedder, E. (1951), Low temperature liquid immiscibility in the system K_2O-FeO-Al_2O_3-SiO_2, *Am. Mineral.*, *36*, 282–286.

Roedder, E. (1978), Silicate liquid immiscibility in magmas and in the system K_2O-FeO-Al_2O_3-SiO_2: An example of serendipity, *Geochim. Cosmochim. Acta*, *42*, 1597–1617.

Roedder, E. (1979), Silicate liquid immiscibility in magmas, in *The Evolution of the Igneous Rocks Fiftieth Anniversary Perspectives*, edited by H. S. Yoder Jr., pp. 15–57, Princeton Univ. Press, Princeton, New Jersey.

Roedder, E., and P. W. Weiblen (1970), Silicate liquid immiscibility in lunar magmas, evidenced by melt inclusions in lunar rocks, *Science*, *167*, 641–643.

Ryerson, F. J., and P. C. Hess (1978), Implications of liquid-liquid distribution coefficients to mineral-liquid partitioning, *Geochim. Cosmochim. Acta*, *42*, 921–932.

Shellnutt, J. G., and Y. Iizuka (2011), Mineralogy from three peralkaline granitic plutons of the Late Permian Emeishan large igneous province (SW China): Evidence for contrasting magmatic conditions of A-type granitoids, *Eur. J. Mineral.*, *23*, 45–61.

Shellnutt, J. G., K.-L. Wang, G. F. Zellmer, Y. Iizuka, B.-M. Jahn, K.-N. Pang, L. Qi, and M.-F. Zhou (2011), Three Fe-Ti oxide ore-bearing gabbro-granitoid complexes in the Panxi region of the Emeishan large igneous province, SW China, *Am. J. Sci.*, *311*, 773–812.

Sisson, T. W. and T. L. Grove (1993), Experimental investigations of the role of H_2O in calc-alkaline differentiation and subduction zone magmatism, *Contrib. Mineral. Petrol.*, *113*, 143–166.

Smith, P. M., and P. D. Asimow (2005), Adiabat_1ph: A new public front-end to the MELTS, pMELTS, and pHMELTS models, *Geochem. Geophys. Geosyst.*, *6*, Q02004, doi: 10.1029/2004GC000816.

Sun, S. S., and W. F. McDonough (1989), Chemical and isotopic systematics of oceanic basalts: Implications for mantle composition and processes, in *Magmatism in the Ocean Basins*, vol. *42*, edited by A. D. Saunders and M. J. Norry, pp. 313–435, Geol. Soc. London. Spec. Publ., Oxford, UK.

Toplis, M. J., and M. R. Carroll (1995), An experimental study of the influence of oxygen fugacity of Fe-Ti oxide stability, phase relations, and mineral-melt equilibria in ferro-basaltic systems, *J. Petrol.*, *36*, 1137–1170.

Veksler, I. V., A. M. Dorfman, L. V. Danyushevsky, J. K. Jakobsen, and D. B. Dingwell (2006), Immiscible silicate liquid partition coefficients: Implications for crystal-melt element partitioning and basalt petrogenesis, *Contrib. Mineral. Petrol.*, *152*, 685–702.

Veksler, I. V., A. M. Dorfman, A. A. Borisov, R. Wirth, and D. B. Dingwell (2007), Liquid immiscibility and the evolution of basaltic magma, *J. Petrol.*, *48*, 2187–2210.

Vicenzi, E., T. Green, and S. Sie (1994), Effect of oxygen fugacity on trace-element partitioning between immiscible silicate melts at atmospheric pressure: A proton and electron microprobe study, *Chem. Geol.*, *117*, 355–360.

Visser, W., and A. F. K. van Groos (1979), Effects of P_2O_5 and TiO_2 on liquid-liquid equilibria in the system K_2O-FeO-Al_2O_3-SiO_2, *Am. J. Sci.*, *279*, 970–988.

Waston, E. B. (1976), Two-liquid partition coefficients: Experimental data and geochemical implications, *Contrib. Mineral. Petrol.*, *56*, 119–134.

Yoder, H. S. (1973), Contemporaneous basaltic and rhyolitic magmas, *Am. Mineral.*, *58*, 153–171.

Zhou, M.-F., W. T. Chen, C. Y. Wang, S. A. Prevec, P. P. Liu, and G. H. Howarth (2013), Two stages of immiscible liquid separation in the formation of Panzhihua-type Fe-Ti-V oxide deposits, SW China, *Geosci. Front.*, *4*(5), 481–502, doi: 10.1016/j.gf.f.2013.04.006.